

Atomic Force Microscopy as a tool for unravelling the relationship between morphology and growth dynamics of organic semiconductors

M. Campione*, M. Moret, and A. Sassella

Department of Materials Science, Università di Milano Bicocca, Via R. Cozzi 53, I-20125 Milano, Italy

Organic semiconductors represent an emerging class of materials which recently has received a huge interest on behalf of a worldwide research community, while finding some applications in alternative and low-cost electronic devices. The performance of an organic semiconductor, in terms of, e.g., charge transport, light emission, and second harmonic generation, depends strongly on its crystallinity and purity. Defect formation in crystals is a key event making growth possible under near-equilibrium conditions. In this work, the morphological study performed by atomic force microscopy of the surface of single crystals and crystalline thin films of organic semiconductors grown under different conditions is presented. It is shown how to exploit the morphological features of defects in order to deduce the molecular orientation within the crystalline samples. Finally, comparison of the crystal structure as determined from X-ray diffraction with results obtained on real crystals is shown to allow the discovery of twins, polytypes, and polymorphs, depending on the growth conditions and mechanisms.

Keywords single crystal, atomic force microscopy, extended defects, crystal growth.

1. Introduction

Since invention of Scanning Tunnelling Microscopy (STM) in the early 1980s [1], new scanning probe microscopies (SPM, see Fig. 1) have been developed [2] and constantly improved, becoming a fundamental tool for research in the field of materials science and, in general, of surface science. In particular, since the very beginning of STM, inorganic semiconductors were particularly blessed by SPM's performance. In the last two decades an increasing interest has grown around organic molecular semiconductors and their potential applications for molecular electronics [3]. This is evidenced both by electronics companies, which start exploiting this class of materials, and by the relevant number of studies undertaken by academic research groups. Today, 25 years after the SPM breakthrough, atomic force microscopy (AFM) can still provide interesting new insights about molecular materials by imaging the surface micro-topography of thin films and single crystals. π -Conjugated molecules are intensively studied as promising organic semiconductors, their thorough study, in particular oligoacenes and oligothiophenes, being pursued by several groups worldwide [4,5].

The physical properties of organic semiconductors (e.g. charge transport and optical properties) rely on intrinsic molecular properties as well as on long range order of their crystalline state. Since organic materials can be employed both as single crystals and crystalline thin films, care must be taken to produce high quality samples. Unfortunately, even with a thorough optimization of specific growth techniques (physical vapour transport, vacuum sublimation, floating drop method, molecular beam deposition, etc) [6-8], crystal growth mechanisms can lead to formation of extended defects which eventually affect the physical properties of a significant part or, in the worst case, even the whole volume of the material. Aside from spectroscopic and diffractometric techniques, recognition and analysis of surface patterns on organic crystalline materials by means of optical and atomic force microscopy, lead us to find out polymorphic-polytypic transitions arising from periodic polysynthetic twinning [9]. Recent findings on quater- (4T) and sexi-thiophene (6T) single crystals and on homo- and hetero-epitaxial thin films obtained with these materials are discussed here, showing that spiral growth patterns observed on

* Corresponding author: e-mail: marcello.campione@mater.unimib.it, Fax: +30 0264485400

the sample crystal surface can be used to reveal and rationalize anomalies in the stacking of molecular layers, found both in bulk samples and in submonolayer films.

2. Experimental procedures

Crystals of the low temperature polymorphs of 4T (4T/LT [10]) and the low and high temperature polymorphs of 6T (6T/LT [11] and 6T/HT [12]) were grown with the floating drop (FD) technique [7] or by physical vapour transport (PVT) [6], and made to adhere to amorphous silica substrates.

Thin films were grown under ultra-high vacuum conditions by organic-MBE (OMBE) [8] at a base pressure below 5×10^{-10} Torr, with a Knudsen type effusion cell with double heater and temperature control. Since OMBE permits a fine tuning of the growth conditions, and therefore of the sample properties, in Fig. 1 all the parameters which can be controlled in our apparatus for such a tuning are sketched. After the choice of starting materials (molecules and substrates), the conditions of the substrate surface, its temperature, and its degree of crystallinity may induce a different growth mode; for example, a low substrate temperature limits diffusion of the molecules on the surface, giving rise to high densities of small nuclei. On the other hand, surfaces with a precise orientation and structure or the application of external fields may favor a unique orientation of the growing islands, possibly leading to epitaxy [13]. As for the source and beam, a higher deposition temperature T_1 increases the beam density and the deposition rate (the temperature T_2 close to the effusion orifice of the Knudsen cell plays a limited role), while the design itself of the source (materials, size of each elements, distance from the substrate) determines the thermodynamics and kinetics of the growth process [14].

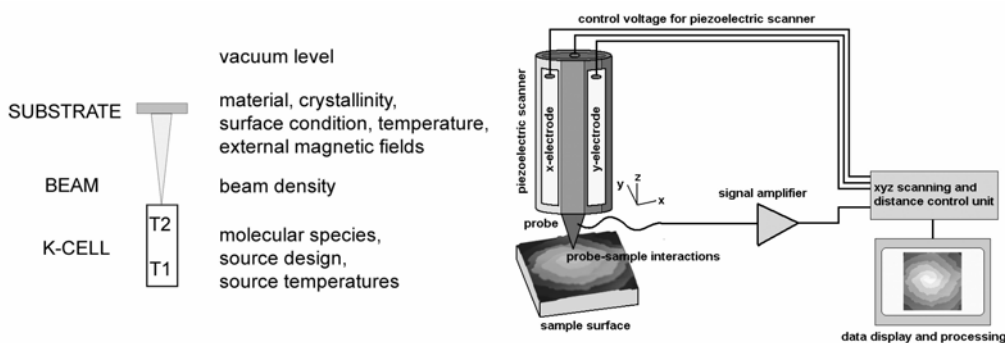


Fig. 1 Sketch of the three main elements for an OMBE experiment (left), with the list of the parameters and conditions which can be tuned for the control of the growth, and schematic representation of the principal components of a Scanning Probe Microscope (right).

The molecular species selected for the present study were 4T and 6T; the substrates were single crystalline 4T and 6T; the deposition temperatures were: $T_1 = 160$ °C for 4T and $T_1 = 290$ °C for 6T and the temperatures T_2 at the effusion orifice were about 10 °C higher than the corresponding T_1 ; the substrate was kept at room temperature. A constant 0.3 nm min^{-1} deposition rate, i.e. a constant beam density, was maintained during growth for all films, constantly monitored by a calibrated quartz microbalance [15].

AFM images were collected in Tapping™ mode, using single beam silicon cantilevers with nominal force constant of 40 N/m and resonance frequency of 300 kHz with a Multimode IIIa AFM (Digital Instruments, Veeco).

3. Results and discussion

3.1 Microtopographic features on the crystal surfaces of 4T and 6T

Single crystals prepared with the FD or PVT techniques sometimes exhibit anomalous surface features indicative of the presence of extended defects. Crystals are self-nucleated from the starting mother solution (FD) or from the inert gas vapour phase (PVT) and subsequently enlarged at low supersaturation with isothermal solvent evaporation or vapour transport, respectively. Under these conditions crystal growth is ruled by dislocation lines with screw components orthogonal to the crystal surface that give rise to lateral advancement of steps through the classical spiral growth BCF mechanism [16]. In the case of oligothiophenes single crystals, surface features are the fingerprint of the role played by mechanisms active during growth. Figure 2a shows a polygonized growth spiral centred at the emergence point of a screw dislocation with steps running parallel to $\langle 100 \rangle$ and $\langle 110 \rangle$ and covering the (001) face of a 4T/LT crystal $\sim 1 \mu\text{m}$ thick. This result fully agrees with crystal growth at low supersaturation where no 2D nuclei can develop. A closer inspection of steps pattern shows that this morphology is incompatible with a regular stacking of the basic monomolecular d_{002} layer along the [001] direction, as required by space group $P2_1/c$ [10]. In general, unsubstituted oligothiophenes share a herringbone packing of molecules giving rise to 2D lamellae (e.g. the d_{002} slice of 4T/LT) [3,17] with the long molecular axis tilted in the same direction by $\sim 65^\circ$ to the lamella. As shown in Figure 2a, the spiral exhibits a characteristic step interlacing [18,19], i.e. pairing and dissociation of step ledges, occurring twice for each turn of the spiral arms and producing a zigzag pattern. This necessarily implies an alternate A/B sequence of macrosteps/lamellae (Fig. 2c-d) which is associated with a faulted stacking of the d_{002} layers [18-20] arising from the presence of two growth spirals mutually rotated by 180° (Fig. 2b).

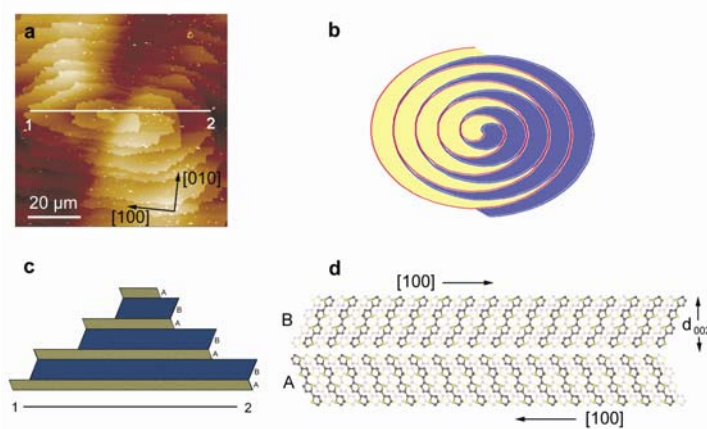


Fig. 2 a) AFM image of a 4T spiral with interlacing steps. b) The two helicoidal macrosteps A and B are self-perpetuated by growing around the screw dislocation core. c) Schematic view of a growth hillock. Normally stacked and faulted macrosteps have, generally, different thicknesses. Due to tilting of 4T molecules with respect to the (001) plane and the 180° mutual rotation of A and B macrosteps, ledges expose re-entrant angles at the common fronts originating from step advancement anisotropy. d) Faulted stacks of 4T/LT as viewed along the [010] direction.

Step height measurements from AFM data of the growth hillock of Fig. 2a, comprising two spirals of the same sign emerging from the same screw dislocation, indicate very large Burgers vectors of $\sim 18 \text{ nm}$ and $\sim 36 \text{ nm}$ for the two spirals, corresponding to ca. 12 and 24 monomolecular layers, respectively. The overall periodicity along [001] becomes then $\sim 54 \text{ nm}$, whilst the correct $P2_1/c$ unit cell periodicity, corresponding to two monomolecular layers, is 3.05 nm [10].

Interlacing of steps occurs because the bunch of layers belonging to the two spirals are mutually rotated through an angle $\Phi = 180^\circ$ about the normal to the (001) face (Fig. 2b). The (monoclinic) anisotropy of step advancement rate within the (001) plane and along different crystallographic directions causes faster moving steps to catch up with the slower underlying ones producing common fronts outside the zigzag. Microscopic observation of interlacing of steps reveals that within the same “single” crystal growth domains generated by different dislocation sources possess different stacking

sequences of the basic d_{002} slice and, hence, a different unit cell vector orthogonal to the face and interaxial angle. The limiting case for 4T/LT, where the two revolving spirals have the same thickness, corresponds to an orthorhombic polytype with $\beta = 90^\circ$.

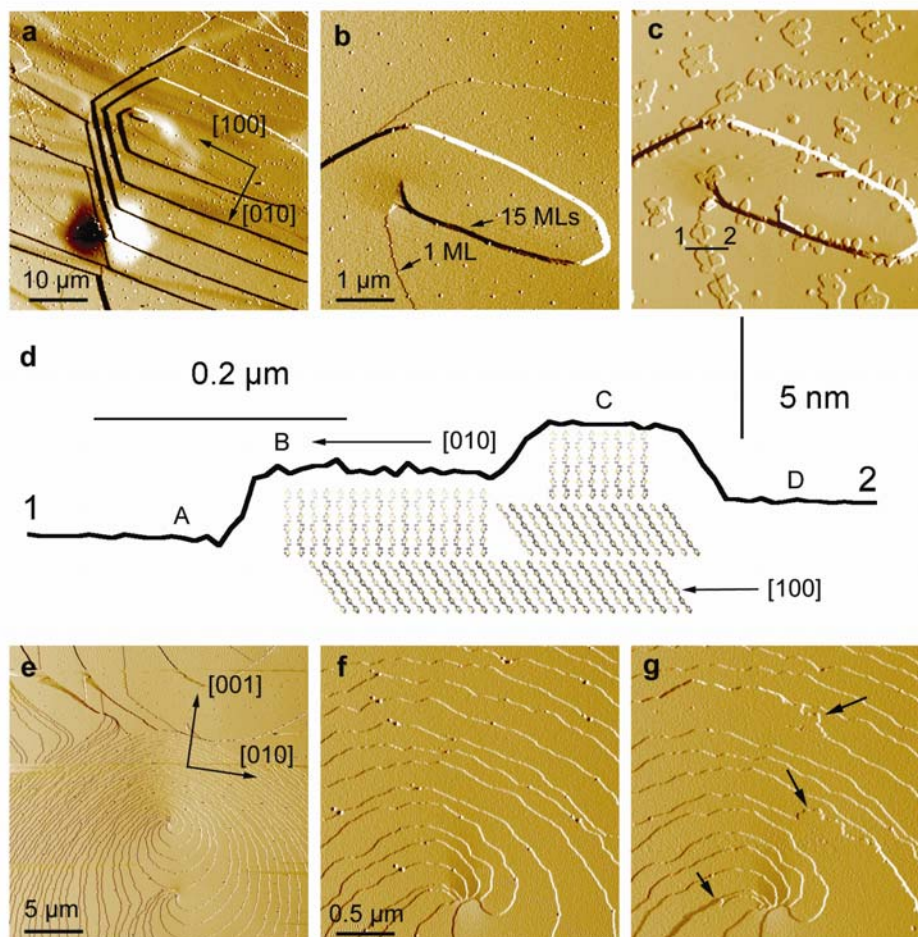


Fig. 3 a) AFM image of a growth spiral on the (001) surface of 6T/HT; the directions of the surface crystallographic axes are indicated. b) Zoomed AFM image of the origin of the spiral imaged in a), with indication of the number of monolayers (MLs) composing the visualised steps. c) Same area as in b) after the deposition of a submonolayer 6T film. d) Cross-sectional profile taken along the black segment between point 1 and 2 in panel c), and structural model deduced from the profile. e) AFM image of growth spirals on the (100) surface of a single crystal of 6T/LT. f) Zoomed AFM image of the growth spiral at the centre of the image in panel e). g) Same area as f) after the deposition of a submonolayer 6T film. Black arrows indicate regions of step-flow growth.

A similar behaviour is found in 6T single crystals. Fig. 3a and b give an example of steps interlacing in a growth spiral on the (001) face of 6T/HT: a monomolecular step (thickness ~ 2.2 nm) is interlaced with a macrostep 33 nm thick (corresponding to ca. 15 monolayers). On the contrary, step interlacing is absent in the complex growth spiral visualized in Fig. 3e and 3f belonging to the (100) face of a single crystal of 6T/LT.

The anomalous stacking of steps, each of them built from one or more elementary lamellae stacked according to the correct space group symmetry, corresponds to periodic polysynthetic twinning and is associated with complex long period polytypism [20]. Rotation of 180° about the normal to the surface of each step with respect to the next and previous ones generates alternating layers of molecules tilted to

the right or to the left, as exemplified by viewing the 4T/LT crystal structure down the [010] direction (Fig. 2d). Each polytype has a period along the normal to the crystallographic plane of the lamella given by the sum ($p+q$) of p monomolecular layers stacked with the same orientation plus the q monomolecular layers (all with the same relative orientation) rotated by 180° with respect to the preceding and following p layers. The polytype period ($p+q$) equals the length of the Burgers vector of the screw dislocation generating the step interlacing [9].

The anomalous interfaces arising between adjacent rotated steps can be realized without significant energy costs because the faulted orientation causes only a small loss of inter-lamella attractive energy, which in the case of 4T/LT has been estimated of the order of 7% [9]. Owing to the strict similarities among the crystal structures of 4T and 6T, this result can be confidently extended to all their polymorphs. Appearance of periodic polysynthetic twinning in lamellar systems is a phenomenon since long known [20,21] and is connected to the formation of twinned nuclei (2D or 3D) on a pre-existing crystal face. For these nuclei, the small interface energy loss assures a significant nucleation frequency, followed by crystal growth due to emerging screw dislocations with large Burgers vectors, cooperating with the correctly oriented layers to originate the long period polysynthetic twins.

3.2 Microtopographic features on the surface of homoepitaxial and heteroepitaxial thin films of 4T and 6T

When nucleation occurs through a 2D mechanism, screw dislocations are no longer necessary for crystal growth [16]. In homo- and hetero-epitaxial growth, 2D nucleation is often a desirable event, since it represents a necessary condition for layer-by-layer growth, which ensures the best quality of interfaces and a control on the amount of deposited material at a molecular scale. For our systems the growth dynamics has been deduced by a morphological investigation carried out on single 2D islands, when the first monolayer is not yet completed. An example of homoepitaxial growth carried out on 6T single crystals is reported in Fig. 3c and g, using as substrate the high and low temperature polymorph, respectively. Important structural information is inferred from the analysis of the morphology of submonolayer films, by imaging the same substrate area before and after deposition (compare Fig. 3b-c and Fig. 3f-g). In both cases, monomolecular islands are nucleated at elemental steps and macrosteps spreading out from growth spirals, but important features differentiate the behaviour of the two polymorphs. On the high temperature polymorph (Fig. 3c), monomolecular islands are observed to have a thickness larger than the elemental step; indeed the profile reported in Fig. 3d shows that the height of the island at the lower substrate terrace (level B), is higher than the level of the upper terrace (level D). This indicates that the structures of adsorbed film and of substrate are different. This difference is ascribed to a smaller tilt angle of 6T molecules of the film phase. This gives rise to the formation of a new step (whose height corresponds to a fraction of the 6T molecule length) which acts as a preferential adsorption site for molecules migrating on the upper terrace. Then, another monomolecular island is nucleated on the upper terrace at the new step. This explains the four levels (A, B, C, and D) evidenced in the cross-sectional profile cutting the elemental step (Fig. 3d). On the other hand, when observing Fig. 3g, one realizes that the homoepitaxial layer (black arrows) deposited on the low temperature polymorph perfectly merges with the elemental steps. This indicates a coincidence between the structure of the film phase and that of the bulk. On the basis of this observation, in the structural model sketched in Fig. 3d, the film phase is represented with the structure of the low temperature polymorph, with domains rotated by 90° around the contact plane normal. Indeed, this azimuthal configuration ensures the minimum lattice mismatch between the low and high temperature polymorphs.

Despite the presence of extended defects on the surface of 4T and 6T single crystals, large domains (of the order of hundreds of micrometers) present defect-free, molecularly flat areas. This low-corrugated surfaces are a perfectly suitable substrate for epitaxial experiments in which the role of homogeneous nucleation (i.e. due to collisions at random sites) is investigated. Fig. 4 shows the morphology of heteroepitaxial 4T islands grown on the (100) surface of 6T/LT. As shown in the cross-sectional profile, all islands have the same thickness. The average thickness of islands (1.5 nm) compares well with the

interlayer spacing of bulk 4T (1.526 nm), indicating that each island is monomolecular with molecules tilted by 65° to the substrate plane (see Fig. 2d). Referring to the equilibrium structures of the two materials (in the low temperature phase), their lattice mismatch is lower than 1%. This value indicates a commensurate epitaxial relation for these organic systems. The structural model deduced from the morphological characteristics of the epilayer is sketched in Fig. 4c. On the basis of symmetry considerations, the presence of two rotational domains must be considered, equivalent by a rotation of 180° around the surface normal.

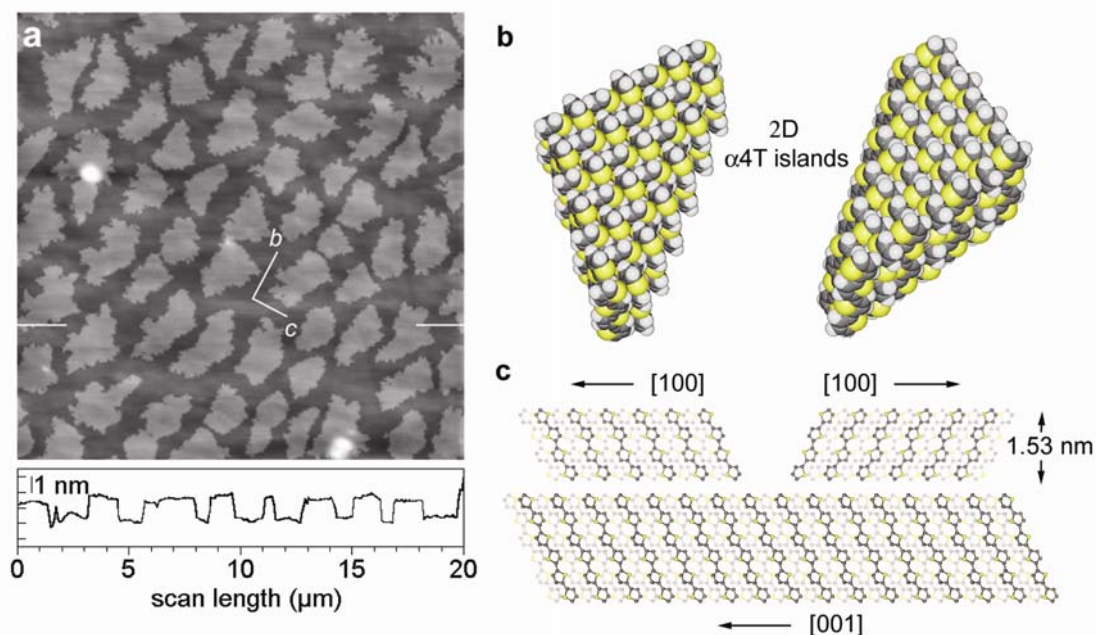


Fig. 4 a) AFM image of a submonolayer film of 4T deposited on the (100) surface of 6T/LT and cross-sectional profile taken along the line connecting the white segments. Substrate surface unit cell axes are indicated in the image. b) Structural model for the triangular islands observed in a). c) Structural model of epitaxial 4T islands showing the epitaxial relation between substrate and overlayer.

The same symmetry arguments hold for the distribution of the growth rates at the edges of the domains, and then for the ultimate shape of the domains. This is indeed observed in the AFM image of Fig. 4a, where islands bounded by the $\langle 110 \rangle$ and $\langle 010 \rangle$ edges (Fig. 4b), giving the domain a shape of an isosceles triangle, appear in two configurations, one rotated by 180° to the other.

If we invert the epitaxial experiment, by depositing 6T on the (001) surface of a single crystal of 4T/LT, the result is that shown in Fig. 5. The cross-sectional profiles reported in Fig. 5a and b reveal islands with homogeneous height of about 2 nm, similar to those observed in the homoepitaxial layer of Fig. 3. This is in accordance with the structural arrangement sketched in Fig. 5c, where the same epitaxial relation for the 4T/6T system is assumed. A deeper observation of the morphology of the islands in Fig. 5a allows to realize that almost all islands present second layer nucleation.

Moreover, the centroids of islands appear with very bright contrast, indicating the presence of a three-dimensional domain. These domains evolve with film coverage to needle-like crystallites, visualised as white segments in Fig. 5b, where a film grown with a double amount of 6T is shown. For rod-like molecules, a needle-like morphology is indicative of crystallites where molecules are arranged with their major axes parallel to the substrate surface (Fig. 5e) [13]. In this arrangement, the strongest interactions among molecules act orthogonally to the substrate surface and in one direction parallel to the substrate plane. This confers the elongated shape to these crystallites. The shape of two-dimensional 6T islands

evolve with film coverage to a well-defined rhombic aspect, indicative of domains bounded by $\langle 011 \rangle$ edges, as sketched in Fig. 5d.

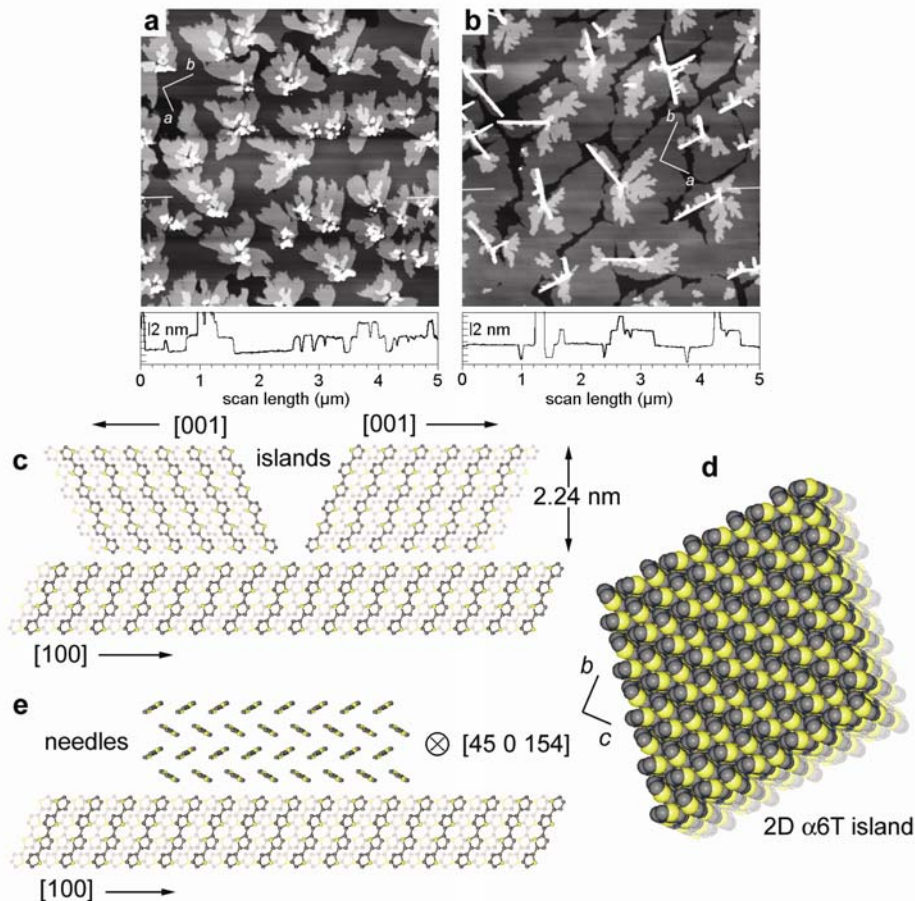


Fig. 5 a) AFM image of a submonolayer 6T film deposited on the (001) surface of 4T/LT and cross-sectional profile taken along the line connecting the white segments. Substrate surface unit cell axes are indicated in the image. b) Same as a) but for a film with a double quantity of deposited material. c) Structural model for the epitaxial islands of 6T on 4T. d) Top view of a polygonal epitaxial island of 6T bounded by $\langle 011 \rangle$ edges (hydrogen atoms are omitted). e) Structural model for the needle-like crystallites observed in b); the direction of the molecular axes (line connecting α and ω C-atoms) is parallel to $[45\ 0\ 154]$ for 6T/LT.

The differences that come to light by a comparison of Figs. 4 and 5, give qualitative indications on the different role played by the microscopic growth events occurring in OMBE experiments. One observes that when 6T is deposited on 4T, second layer nucleation occurs almost simultaneously to first layer; moreover 3D aggregates coexist with 2D epitaxial islands. These events do not occur when 4T is deposited on 6T. These observations are the direct consequence of the higher molecular mass of 6T with respect to 4T. Indeed, when molecules are deposited on the substrate, they start migrating, assuming a flat-lying configuration. In this configuration, 6T molecules are more bonded to the substrate surface than 4T molecules. This has two effects: i) the nucleation of domains with flat-lying molecules is favoured, and ii) energy barriers associated to interlayer diffusion are higher. Condition i) is responsible for the formation of 3D aggregates that evolve with coverage to needle-like crystallites, whereas condition ii) increases the density of molecules on the surface of 2D islands, inducing second layer nucleation.

4. Conclusions

The high accuracy and resolution of AFM makes this technique suitable for the study of the morphology-structure relationship, from bulk samples to submonolayer scales. The unravelling of this relationship is the first step to the analysis of the growth dynamics of crystalline aggregates. Organic semiconductors are characterized by a relatively low symmetry of the growth units, and this originates a huge variety of defect configurations which are reminiscent of the mechanisms of aggregation of molecules. It was shown that the morphological features of extended defects, such as screw dislocations emerging from molecularly flat surfaces, if analysed on the light of the knowledge of the equilibrium crystal structure of the material, reveal the presence of twins, polymorphs, and polytypes in crystal nucleated by a 3D mechanism. When a 2D mechanism of nucleation is involved, the analysis must rely on the morphology of stable monomolecular islands. The height and shape of stable 2D islands can suggest univocally the molecular orientation, which must be consistent with symmetry constraints.

It is worth mentioning that some morphological details which would be very useful for the present study are not yet thoroughly accessible in modern AFM instruments. For instance, the accurate measurement of re-entrant angles at the edges of 2D and 3D crystalline aggregates would allow to determine the polarity of the crystallographic axes (e.g. the *a*-axis of 4T/LT and 6T/HT).

Acknowledgements A. Papagni, A. Borghesi, and S. Caprioli are gratefully acknowledged for their support.

References

- [1] G. Binnig and H. Rohrer, *Helv. Phys. Acta* **55**, 726 (1982).
- [2] G. Binnig, C.F. Quate, and C. Gerber *Phys. Rev. Lett.* **56**, 930 (1986).
- [3] D. Fichou, *J. Mater. Chem.* **10**, 571 (2000).
- [4] M. Bendikov, F. Wudl, and D. F. Perepichka, *Chem. Rev.* **104**, 4891 (2004).
- [5] J.-L. Brédas, D. Beljonne, V. Coropceanu, and J. Cornil, *Chem. Rev.* **104**, 4971 (2004).
- [6] R. A. Laudise, C. Kloc, P. G. Simpkins, and T. Siegrist, *J. Cryst. Growth* **187**, 449 (1998).
- [7] M. Campione, R. Ruggerone, S. Tavazzi, and M. Moret, *J. Mater. Chem.* **15**, 2437 (2005).
- [8] S.R. Forrest, *Chem. Rev.* **97**, 1793 (1997).
- [9] M. Moret, M. Campione, L. Raimondo, A. Sassella, S.Tavazzi, and D. Aquilano *Phys. Stat. Sol. C* **4**, 711 (2007).
- [10] T. Siegrist, C. Kloc, R. A. Laudise, H. E. Katz, and R. C. Haddon, *Adv. Mater.* **10**, 379 (1998).
- [11] G. Horowitz, B. Bachet, A. Yassar, P. Lang, F. Demanze, J.-L. Fave, and F. Garnier, *Chem. Mater.* **7**, 1337 (1995).
- [12] T. Siegrist, R.M. Fleming, R.C. Haddon, R.A. Laudise, A.J. Lovinger, H.E. Katz, P.D. Bridenbaugh, and D. Davis, *J. Mater. Res.* **10**, 2170 (1995).
- [13] M. Campione, A. Sassella, M. Moret, A. Papagni, S. Trabattoni, R. Resel, O. Lengyel, V. Marcon, and G. Raos, *J. Am. Chem. Soc.* **128**, 13378 (2006).
- [14] A. Sassella, M. Campione, A. Papagni, C. Goletti, G. Bussetti, P. Chiaradia, V. Marcon, and G. Raos, *Chem. Phys.* **325**, 193 (2006).
- [15] M. Campione, M. Cartotti, E. Pinotti, A. Sassella, and A. Borghesi, *J. Vac. Sci. Technol. A* **22**, 482 (2004).
- [16] W. K. Burton, N. Cabrera and F. C. Frank, *Phil. Mag.* **243**, 299 (1951).
- [17] M. Moret, M. Campione, A. Borghesi, L. Miozzo, A. Sassella, S. Trabattoni, B. Lotz and A. Thierry, *J. Mater. Chem.* **15**, 2444 (2005).
- [18] D. Aquilano, L. Pastero, S. Veessler, and J. P. Astier in: *Crystal Growth: from basic to applied*, S.Carrà, and C. Paorici (eds.), (Accademia Nazionale dei Lincei, Roma, 2003), pp. 47-64.
- [19] W. J. P. van Enkevort, and P. Bennema, *Acta Crystallogr., Sect. A* **60**, 532 (2004).
- [20] D. Aquilano, *J. Cryst. Growth* **37**, 215 (1977).
- [21] R. Boistelle, *Defect Structures and Growth Mechanisms of Long-chain Alkanes*, Current Topics in Materials Science, Vol. 4, (North-Holland Publishing Company, 1980), chap. 8.